



Thermal aberrations and structured light II: experimental simulation with DMDs

Stirling Scholes¹ · Andrew Forbes²

Received: 15 January 2021 / Accepted: 28 June 2021 / Published online: 16 July 2021
© The Author(s), under exclusive licence to Springer-Verlag GmbH Germany, part of Springer Nature 2021

Abstract

In part I of this work (Scholes and Forbes, Appl Phys B, 2021. <https://doi.org/10.1007/s00340-021-07657-y>), we provided a general model for optically induced thermal aberrations due to high power structured light pumps, highlighting the implications for arbitrary structured probes. We showed how the thermal effects impact on various structured light fields, and illustrated how to mitigate these effects using the structure of light as a new degree of freedom for control. Here, in part II, we demonstrate that thermo-optical effects can be simulated experimentally with cheap and fast digital micro-mirror devices. This approach represents a fully configurable, versatile, low-power physical simulator which replicates all the salient effects seen with high power sources, the latter notoriously difficult to experiment with. We demonstrate the efficacy of this simulator with various structured light beams under realistic thermal conditions which we programme as phase-only computer generated holograms, effective because the pertinent thermal effects themselves are phase-only aberrations to the field. Our work provides a new means to simulate thermal aberrations due to high power lasers and could be extended to correction techniques too.

1 Introduction

Optically induced thermal effects have been extensively studied to date, both theoretically [1–4] and experimentally [5, 6], motivated by the quest for high power and high brightness laser sources, and the optimal delivery of such beams through optical systems. In part I [7] of this two part article, we provided a comprehensive model of optically induced thermal effects and their concomitant deleterious impact on the optical beam. In particular, the model incorporated both, arbitrary forms of structured light [8] as the pump source in laser systems, and as the delivered beam through optical systems, where the “pump” and “probe” are one and the same. As illustrative examples, we characterised the optically induced thermal effects such as the temperature profile and thermal stress in a optics with both radial and Cartesian symmetries when heated by a variety

of structured light sources, and considered the reciprocal thermally induced optical effects, including a full aberration treatment to deduce the phase distortion and its impact on the structured light beam.

Given that thermally induced optical aberrations are predominantly observed in high power applications and take effect over short time scales, experimental verification is challenging and always limited to very specific test cases, most often high power Gaussian beams passing through some medium (optical windows for example) or solid-state lasers that output high power beams but suffer from thermal effects in the gain medium. Numerous approaches have been used to measure thermal aberrations both inside and external to lasers, including simple power monitoring [9], interferometric methods [10–14], lens-based methods [15–17], and techniques using specialised equipment such as Shack–Hartman wavefront sensors [18–21]. Together with advances in measurement has been advances in aberration correction, most notably with adaptive optics [22–24]. However, high power laser studies involving the impact of thermal aberrations on structured light fields and the mitigation thereof remain largely neglected due to the complexity of the experiments. The limited studies include thermal and gain effects on Ince–Gaussian beams [25, 26], Helmholtz–Gaussian beams [27] and Bessel–Gaussian beams [28], as well

✉ Andrew Forbes
Andrew.Forbes@wits.ac.za

¹ Structured Light Group, Physics, University of the Witwatersrand, 1 Jan Smuts Avenue, Johannesburg 2000, South Africa

² School of Physics, University of the Witwatersrand, 1 Jan Smuts Avenue, Johannesburg 2000, South Africa

as some intra-cavity mode control with adaptive optics [29–34]. It has also been demonstrated that annular pump beams could be used to reduce the thermal lensing effect on Gaussian beams passing through the centre of the optic [35, 36]. Such annular pumps have been used to create high power annular structured light fields, for example, cylindrically symmetric vector vortex beams such as radially polarised beams, and the scalar equivalent vortex beams carrying orbital angular momentum [37–41].

Here, we show what we believe to be the first demonstration of a fully configurable, real-time experimental simulator of thermally induced optical aberrations without the need for high laser powers or sources. We make use of a digital micro-mirror device (DMD) programmed with computer generated holograms (CGHs), foregoing the need for specific optical materials and lasers. This is possible, because the reciprocal effect of the medium on the beam is a phase-only perturbation and thus excellently suited to CGH simulation. Here, we employ only a single Spatial Light Modulator (SLM), but the system could be easily extended to simulate multiple optical mediums and multiplane conversion with the use of additional modulators or multiple passes [42]. The flexibility and speed of DMDs allows us to fully map out the parameter space of the models, and to demonstrate the thermal effects in real time. To demonstrate the predictions of part I [7], we implement our experimental simulator using the selection of probe beams and heat sources shown in Fig. 1. Structured light is a highly topical field and describes the ability to tailor light in all its degrees of freedom, opening up a myriad of applications [8, 43–46], and fuelling the development of structured light sources [44], particularly at high powers [47–53]. In parallel, DMDs have been used extensively to create [54–64] and to a lesser extent detect [65–68] structured light fields, and have gained in popularity of late [69]. However, they have yet to be used to simulate perturbing media, and in particular thermally induced optical effects. By doing so, we are able to fully characterise the impact of thermal aberrations on structured light, demonstrating our prior predictions and outlining a robust toolkit for future studies. Although we consider only thermal aberrations here and not polarization distortions due to thermally induced stresses, it is possible to extend the DMD demonstration to cover this too by exploiting its ability to modulate polarization states independently and in real time [70–72].

2 Experimental setup

We constructed the experimental setup depicted conceptually in Fig. 2 to demonstrate the approach covered in the associated theory paper. A TI 3000 DMD with a screen resolution of 608×684 pixels was used to physically

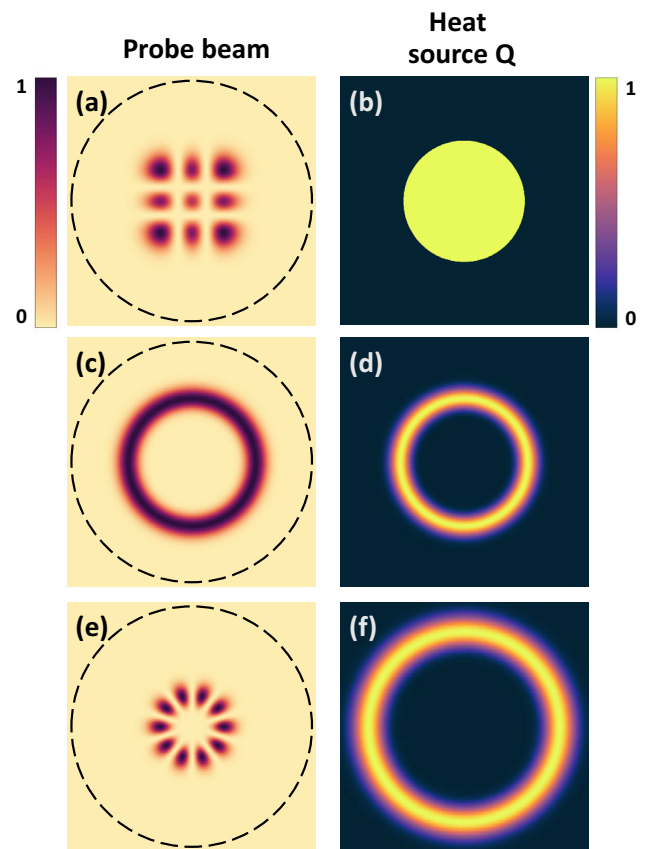


Fig. 1 A selection of heat sources Q and probe beams are used to examine an optical medium under heating. The black dashed lines in the probe beam panels indicate the boundary of the medium being heated. In cases **a** through **d**, the area of the optic being heated and the area illuminated by the probe are the same, whilst in **e** and **f**, the probe beam and heat source are spatially separated. Specifically: **a** a flat-top heat source and **b** HG probe beam; **c**, **d** a $LG_{\ell>0}^0$ heat source and probe beam; **e** a probe beam passing through the centre of the optic, shown here as an LG superposition and **f** an $LG_{\ell>0}^0$ heat source at the boundary of the optic

simulate a heated optical element. The system is analogous to an old film projector. By displaying an ordered series of holograms where each hologram captures the temperature profile of the optic, beams with a phase $\Omega(x, y)$ and amplitude profile $A(x, y)$ were created as though they had been produced by a high-intensity source. A camera then measured these beams at the focal plane of a lens f_1 , where the phase would effect the intensity. Thus, by changing the holograms, the setup can be easily configured to produce beams which both match the cases presented in the theory, and provide a physical simulacrum to a system experiencing thermal aberrations. Because DMDs are amplitude-only devices, we employ complex amplitude modulation techniques [73, 74] to make it work for amplitude and phase, with the resulting hologram transmission function given by

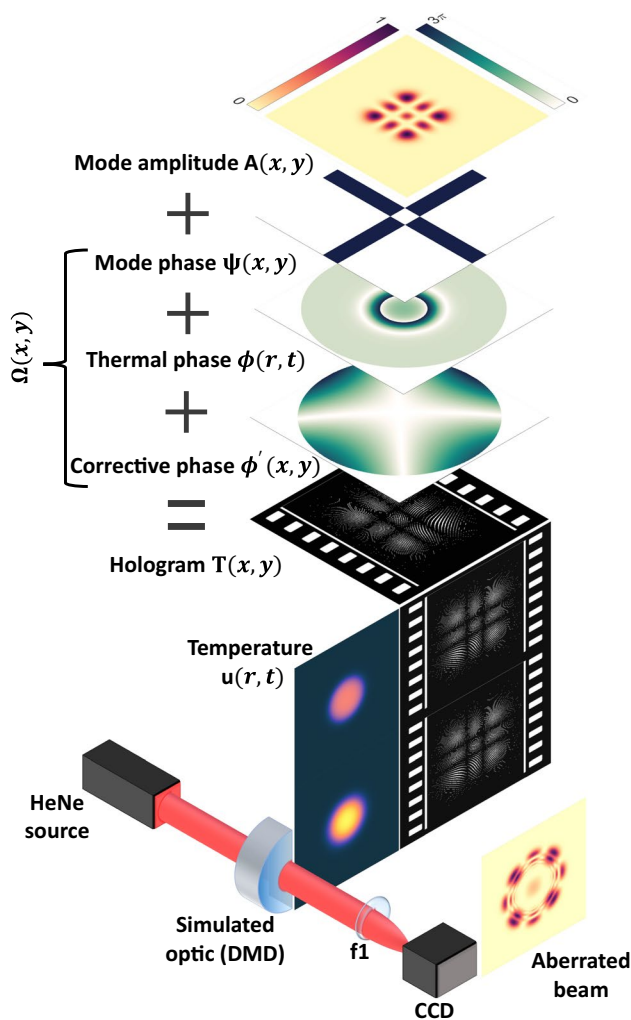


Fig. 2 The experimental setup shown conceptually. We used a DMD as though it was an old film projector, i.e., dynamically simulating the heated optic by displaying an ordered set of holograms corresponding to the temperature profile of the optic. Each hologram encodes an amplitude $A(x, y)$ and a phase, where the total phase $\Omega(x, y)$ is made up of three components: the phase inherent to the desired mode $\psi(x, y)$; the phase of the thermal aberration $\phi(r, t)$, and the corrective phase accounting for the deformations to the DMD $\phi'(x, y)$. A well-expanded and collimated beam from a HeNe source was incident on the DMD. The first-order diffraction from the hologram was filtered by a 4f system (not shown) and recorded at the Fourier plane by a camera

$$T(x, y) = \frac{1}{2} + \frac{1}{2} \text{sign}[\cos(\varphi) - \cos(B)], \tag{1}$$

with

$$\varphi = \Omega(x, y) - 2\pi g(x, y), \tag{2}$$

and

$$B = \arcsin[A(x, y)]. \tag{3}$$

The function $g(x, y)$ is an additional periodic grating encoded into the hologram to spatially separate the desired 1st order diffraction from the natural 0th order of the DMD. This in conjunction with a 4f spatial filtering system allows for the accurate measurement of the modulated beam. The $\text{sign}()$ function binarises the output from the $\text{cos}()$ terms, creating a hologram which can be displayed on the DMD. The DMD was oriented at 12° to the incident beam to maximise efficiency whilst maintaining beam fidelity [69]. To ensure accurate measurement of the effects of the encoded thermal phase $\phi(r, t)$, the phase aberrations inherent to the DMD were accounted for using techniques adapted from those developed for liquid crystal SLMs [69, 75]. These additional aberrations are a consequence of the finite manufacturing tolerances of the DMD as well as the mechanical stresses applied to the screen due to its mounting. Adding a predetermined corrective phase ϕ' to each hologram negates the effect of these additional aberrations [76, 77]. The advantage of verifying the theoretical approach using this experimental system is that it provides a test bed which is highly versatile (i.e., able to generate many test modes quickly) whilst being simple, cheap, and safe to operate in comparison to existing systems for measuring thermal aberrations.

3 Results for a flat-top source

Here, we experimentally simulate on our DMD the effect of heating a Tm:YLF rod with a centrally positioned radially symmetric heat (flat-top) source of uniform intensity. The parameters used for the heat source and the rod are given in Table 1. An HG beam of index 2,2 and waist 3.5×10^{-4} m having the appropriate thermally induced aberration $\phi(r, t)$ was created and measured by the experimental setup in Fig. 2. The thermal aberrations were calculated using the first 100 even Radial Zernike polynomials. For this case, we monitored the degradation of the beam over time as the rod heated for 10 ms to mimic a physically meaningful system in which the thermal load would not result in damage to the rod [78]. Figure 3 shows the measured beam and corresponding phase and temperature profiles at four selected points in time.

At $t = 0$, the modelled rod has a uniform initial temperature distribution and so applies no phase to the beam. Consequently, the measured beam is unaberrated. As the rod heats, it takes on a non-uniform temperature distribution introducing thermal aberrations dominated by a defocus and a primary spherical aberration. These aberrations enlarge the total area of the beam and completely degrade its structure. The results presented in Fig. 3 were selected from a continuous set of measurements spanning

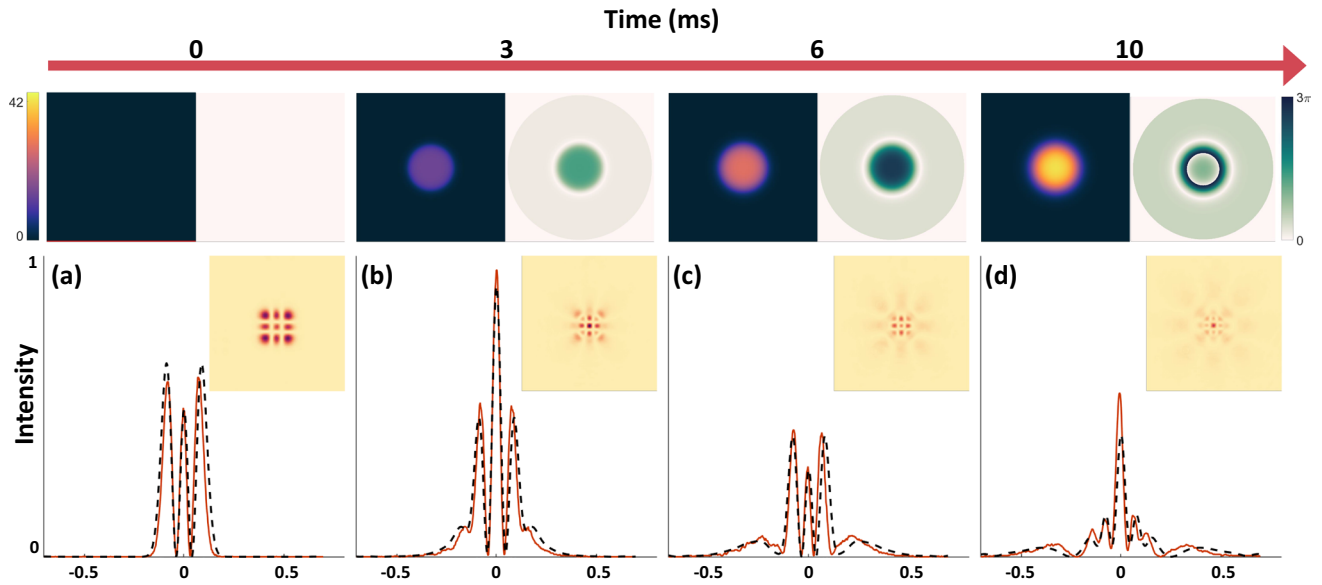


Fig. 3 The effect of a flat-top heat source on an HG probe beam over time. The upper panels show the temperature $u(r, t)$ of the modelled rod and the aberrating phase $\phi(r, t)$ of the hologram. The main panels show the cross sections of the simulated beams and measured beams

as black dashed and orange solid lines, respectively. Measurements are shown at four points in time, **a** at $t = 0$, **b** at $t = 3$, **c** at $t = 6$, and **d** at $t = 10$ ms, respectively. The cross sections are plotted on a transverse axis in millimetres. The insets show the measured beam

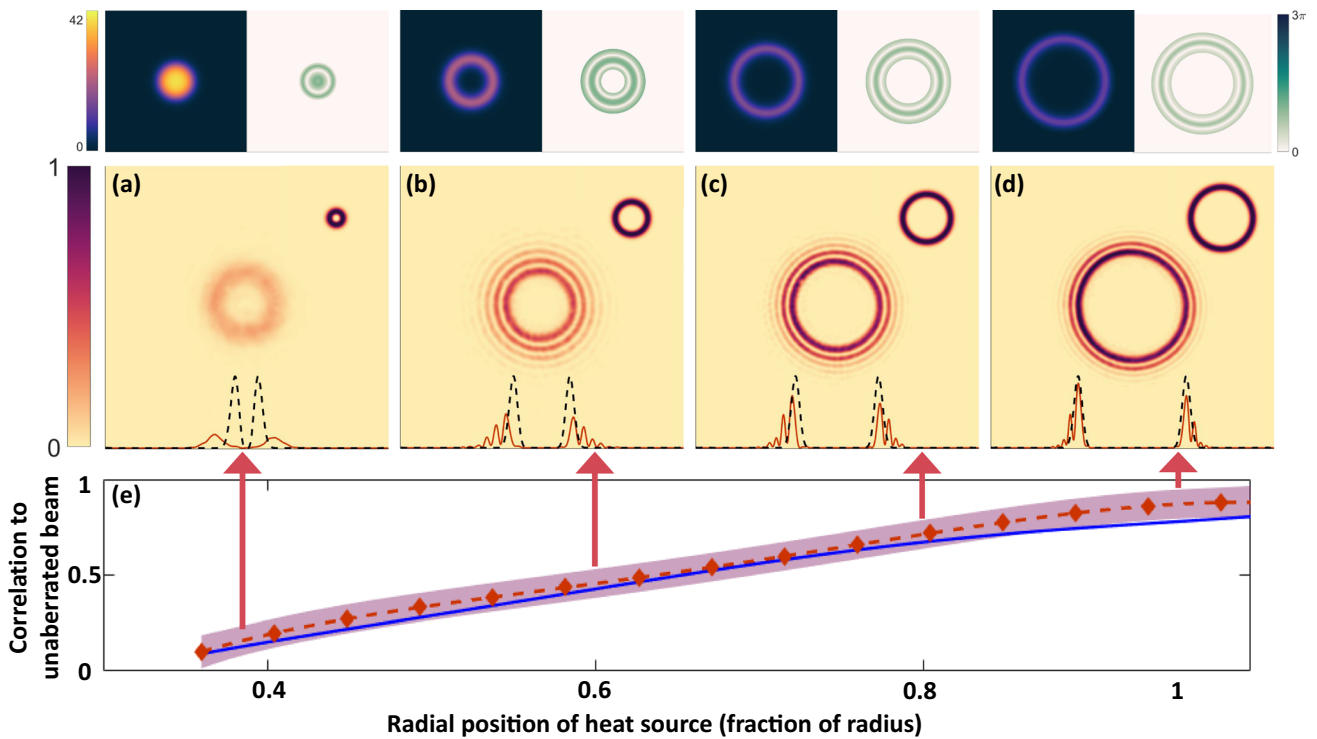


Fig. 4 The self-action of an LG beam. The upper insets show the temperature of the rod $u(r, t)$ and aberrating phase $\phi(r, t)$ of the hologram. Panels **a–d** show the measured beams for an annular source with its outer boundary at $0.36\times$, $0.6\times$, $0.8\times$, and $1\times$ the radius, respectively. The insets in these panels show the input beams. The line plots show the profiles of an unaberrated beam and the measured beams as black dashed and solid orange lines, respectively. Panel **e**

shows the correlation between the measured beam and the simulation of an unaberrated beam as a function of heat source position. The dashed red line indicates the line of best fit for the experimental data with the shaded region indicating the 95% confidence interval. The solid blue line is the theoretical prediction. The half panels depict the phase and temperature profiles of the simulated rod

Table 1 Material constants used in the simulation [78]

Parameter	Value
Heat source radius (m)	470×10^{-6}
Rod radius (m)	1.5×10^{-3}
Rod length (m)	5×10^{-3}
Absorption coefficient (m^{-1})	143
Thermal conductivity ($W m^{-1}K^{-1}$)	7.2
Fractional heat load	0.33
Density ($kg m^{-3}$)	3990
Specific heat capacity ($J kg^{-1}K^{-1}$)	790
Heat source energy (W)	200
Heat source duration (s)	0.01
Refractive index per unit temperature (K^{-1})	-66×10^{-7}

the 10 ms heating time. These as well as the results for subsequent figures are available as .gif files in the supplementary materials.

4 Results for an annular source

4.1 The self-action

The self-action of an annular heat source was observed using an LG beam which had the same parameters as those given in Sect. 3. The LG beam had a waist of 2.5×10^{-4} m and was expanded towards the radius by adjusting its azimuthal index ℓ . The aberrating phase $\phi(r, t)$ imparted to the beam was calculated using the first 100 even Annular Zernike polynomials. Figure 4 shows the measured beam and corresponding aberrating phase $\phi(r, t)$ and temperature $u(r, t)$ distributions for an annular source with its outer boundary at four positions. The measurement at $0.36\times$ the radius corresponds to the minimum size of an annular source

The temperature insets in Fig. 4 show that as the annular heat source moved towards the radius of the modelled rod, an area of uniform temperature distribution formed within the area encompassed by the annulus. However, aberration is still present within the heated annular region. When the beam was near the centre of the rod, a defocus and a primary

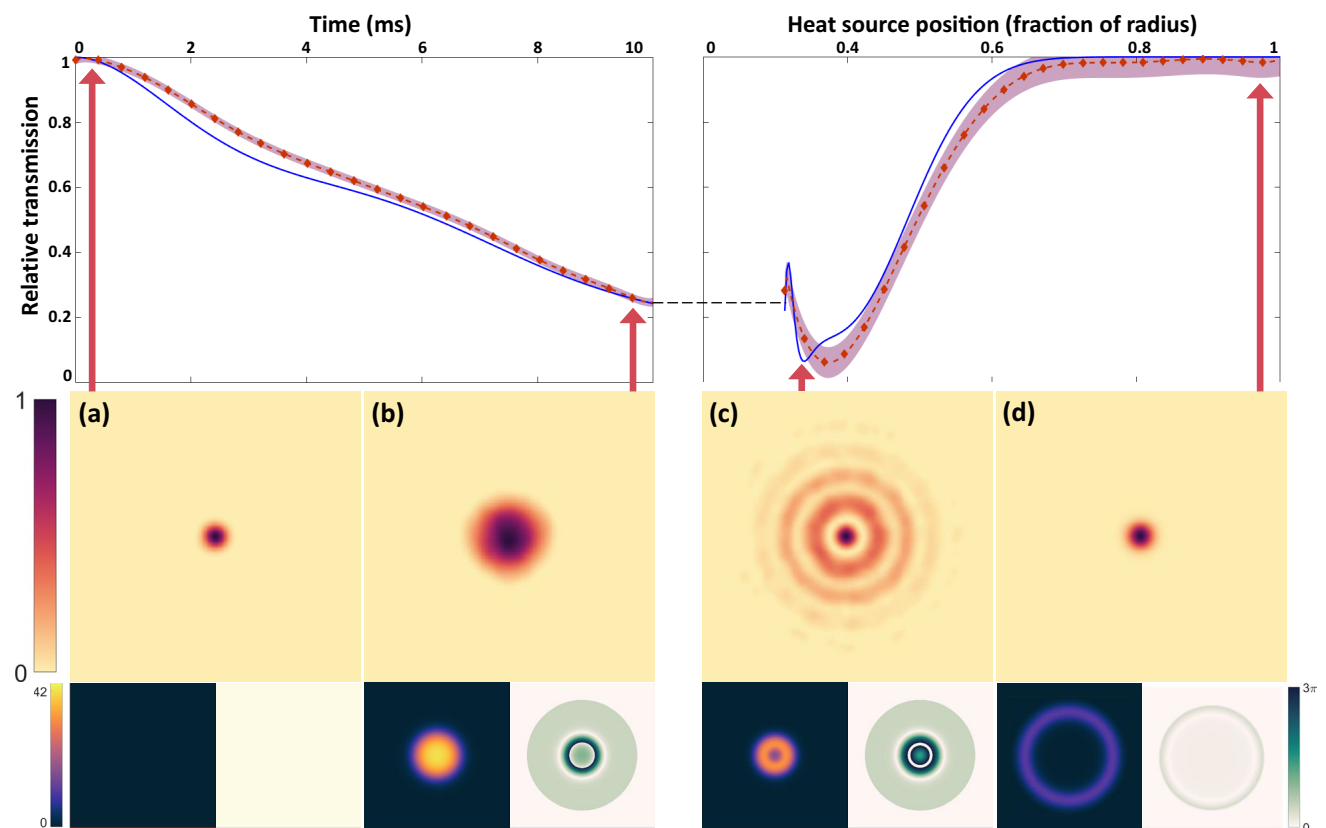


Fig. 5 The intensity through an aperture for a Gaussian beam passing through the modelled rod: over time on the left, and as the annular source moves outward on the right. The dashed red line indicates the line of best fit for the experimental data with the shaded region indicating the 95% confidence interval. The solid blue line is the theo-

retical prediction. The panels **a–d** show the measured beams at the positions indicated by the arrows with the corresponding temperature $u(r, t)$ and aberrating phase $\phi(r, t)$ profiles shown in the half panels below. Note that each measured beam has been independently normalised to aid in visualisation

spherical aberration were dominant. These resulted in both an enlargement of the beam as a whole, and a broadening of its ring structure. This is seen by the large size discrepancy between the profile of the measured beam and the profile of an unaberrated beam shown in panel (a) of Fig. 4. As the annular source moved outwards, more complex aberrations created concentric rings of decreasing intensity around a central high-intensity ring. Most importantly, with the annular ring near the radius of the modelled rod, the aberrations were reduced as a consequence of the reduced temperature gradient in the rod. The result was a reduction in the prevalence of the concentric rings, allowing the inner most ring to approach the correct size and intensity for an unaberrated beam. The reduction in the strength of the aberrations was quantified by calculating the correlation between the measured beam and an unaberrated beam. Figure 4 panel (e) shows this quantity as a function of the position of the outer edge of the heat source. As the heat source moved outwards, the correlation increased from less than 20% to in excess of 80%. This result confirms that even when considering a beam which is spatially coincident with a heated annular region, the thermally induced aberrations are reduced as the heated region approaches the radius.

4.2 Special annular cases

We now consider the special case where probe beams were passed through the centre of the rod, whilst an annular heat source moved outwards from the centre to the radius. To quantify the reduction in thermal aberrations for a realistic physical system, the loss in intensity of an aberrated Gaussian beam of waist 3.5×10^{-4} m passing through an aperture at the focal plane was measured. The aperture was sized at $1/e^2$ the width of an unaberrated beam. The total intensity transmitted through this aperture was then measured, effectively performing a D86 measurement [79–81]. Two measurements were taken. First, to provide a baseline, we used the same parameters as in Sect. 3. As heating occurred, the Gaussian beam passing through the centre of the modelled rod became aberrated and was partially occluded by the aperture, with the corresponding loss in intensity recorded. Second, the same system was fixed at a time of $t = 10$ ms and the increase in intensity measured as an annular heat source moved outwards towards the radius.

The left-hand side of Fig. 5 shows that under realistic circumstances, a Gaussian beam passing through a centrally heated Tm:YLF rod may experience as much as a 75% reduction in aperture transmission at the focal plane. This is due to the thermally induced defocus aberration, the effect of which is clear when comparing the sizes of the beams in panels (a) and (b). This degradation is significant, especially in industrial applications where high beam intensity at specific planes is

required [82–84]. The right-hand side of Fig. 5 shows how as the annular source moved outwards, the aperture transmission increased. The plot depicts the increase in transmission against the position of the outer edge of the heat source as a fraction of the radius. Interestingly, an annular source initially resulted in a reduction in the transmission. This occurred when the annular source was sufficiently near the centre of the rod for the Gaussian beam to overlap with it, resulting in the formation of concentric rings which can be seen in panel (c). These concentric rings moved energy radially outwards resulting in an overall decrease in transmitted intensity. As the annular heat source was moved further outwards, the Gaussian beam was contained entirely within the region of constant phase. Once within this region the beam was unaberrated, thus the relative transmission increased to a value of ≈ 1 .

Importantly, this region of constant phase bounded by the heat source reduces aberrations for all beam types, not only Gaussians. Figure 6 shows the temperature $u(r, t)$ of the rod for an annular source at the radius with the corresponding aberrating phase $\phi(r, t)$ calculated by the Radial Zernike polynomials. Additionally, the figure shows the effect of this phase on superpositions of HG and LG modes passing through the centre of the optic. The high degree of overlap between the profiles of the measured results and the theoretical prediction for an unaberrated beam indicates that even modes which are highly structured can pass undisturbed through the centre of an annular heat source.

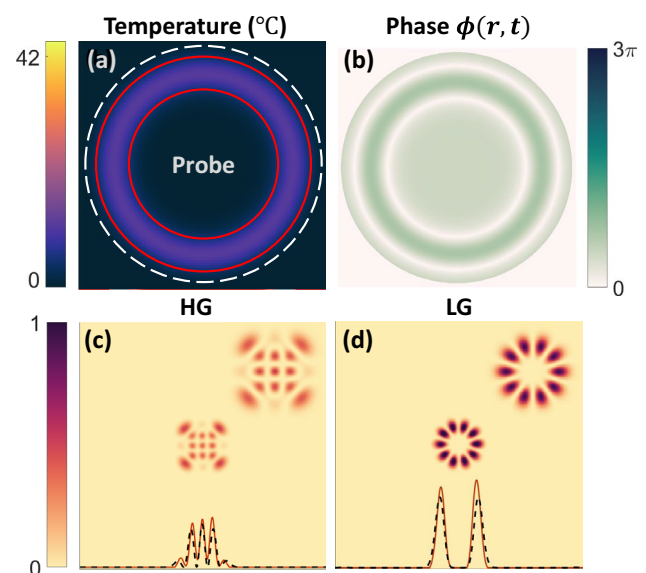


Fig. 6 The special case of an annular heat source with superpositions of HG (c) and LG (d) probe beams. **a** The temperature $u(r, t)$ of the rod for an annular heat source (red lines) at its radius (white dashed line). **b** The aberrating phase $\phi(r, t)$ of the hologram. The insets in c and d show the input beams. The line plots show the profiles of unaberrated beams and the measured beams as black dashed and orange solid lines, respectively

5 Conclusion

In this work, we have presented an experimental simulator built around a DMD which is capable of mimicking thermally induced optical effects in real time and at low power, which we used to experimentally demonstrate the theory presented in part I [7] of this two part series. We used our experimental test bed to simulate various example cases, including a centrally heated optic, an annular heated optic, and non-overlapping pump and probe beams, including superpositions of structured light modes. Not only do we demonstrate the theory of part I [7], but in doing so outline a new toolkit for the study of fast thermal processes in a simple, fast and safe manner.

Acknowledgements We thank the Council of Scientific and Industrial Research with the Department of Science for the funding provided through the Interbursary Incentive Funding Programme (CSIR-DST IBS).

Declarations

Conflict of interest The authors declare no conflict of interest in the production or publication of this work.

References

1. L. Cini, J. Mackenzie, Analytical thermal model for end-pumped solid-state lasers. *Appl. Phys. B* **123**(12), 273 (2017)
2. M.A. Isidro-Ojeda, J.J. Alvarado-Gil, V.S. Zanuto, M.L. Baesso, N.G. Astrath, L.C. Malacarne, Laser induced wavefront distortion in thick-disk material: an analytical description. *Opt. Mater.* **75**, 574–579 (2018)
3. L.C. Malacarne, N.G. Astrath, M.L. Baesso, Unified theoretical model for calculating laser-induced wavefront distortion in optical materials. *JOSA B* **29**(7), 1772–1777 (2012)
4. L.C. Malacarne, N.G. Astrath, L.S. Herculano, Laser-induced wavefront distortion in optical materials: a general model. *JOSA B* **29**(12), 3355–3359 (2012)
5. A.J. Kemp, G.J. Valentine, D. Burns, Progress towards high-power, high-brightness neodymium-based thin-disk lasers. *Prog. Quantum Electron.* **28**(6), 305–344 (2004)
6. M. Bass, W. Koechner, *Solid-state lasers : a graduate text.* (Springer-Verlag, New Haven, 2002). [Online]. <http://www.springer.de/phys/>
7. S. Scholes, A. Forbes, Thermal aberrations and structured light I: analytical model for structured pumps and probes. *Appl. Phys. B* (2021). <https://doi.org/10.1007/s00340-021-07657-y>
8. A. Forbes, M. de Oliveira, M.R. Dennis, Structured light. *Nat. Photon.* **15**, 253–262 (2021)
9. D.-L. Kim, B.-T. Kim, Laser output power losses in ceramic Nd:YAG lasers due to thermal effects. *Optik* **127**(20), 9738–9742 (2016)
10. H. Welling, C.J. Bickart, Spatial and temporal variation of the optical path length in flash-pumped laser rods. *JOSA* **56**(5), 611–618 (1966)
11. G. Baldwin, E. Riedel, Measurements of dynamic optical distortion in Nd-doped glass laser rods. *J. Appl. Phys.* **38**(7), 2726–2738 (1967)
12. J. Bradford, R. Eckardt, Compensating for pump-induced distortion in glass laser rods. *Appl. Opt.* **7**(12), 2418\1-2420 (1968)
13. C. Pfistner, R. Weber, H. Weber, S. Merazzi, R. Gruber, Thermal beam distortions in end-pumped Nd:YAG, Nd:GSGG, and Nd:YLF rods. *IEEE J. Quantum Electron.* **30**(7), 1605–1615 (1994)
14. W. Clarkson, Thermal effects and their mitigation in end-pumped solid-state lasers. *J. Phys. D Appl. Phys.* **34**(16), 2381 (2001)
15. D. Burnham, Simple measurement of thermal lensing effects in laser rods. *Appl. Opt.* **9**(7), 1727–1728 (1970)
16. J. Murray, Pulsed gain and thermal lensing of Nd:LiYF₄. *IEEE J. Quantum Electron.* **19**(4), 488–491 (1983)
17. B. Neuenschwander, R. Weber, H.P. Weber, Determination of the thermal lens in solid-state lasers with stable cavities. *IEEE J. Quantum Electron.* **31**(6), 1082–1087 (1995)
18. P. Hardman, W. Clarkson, G. Friel, M. Pollnau, D. Hanna, Energy-transfer upconversion and thermal lensing in high-power end-pumped Nd:YLF laser crystals. *IEEE J. Quantum Electron.* **35**(4), 647–655 (1999)
19. J.D. Mansell, J. Hennawi, E.K. Gustafson, M.M. Fejer, R.L. Byer, D. Clubley, S. Yoshida, D.H. Reitze, Evaluating the effect of transmissive optic thermal lensing on laser beam quality with a Shack-Hartmann wave-front sensor. *Appl. Opt.* **40**(3), 366–374 (2001)
20. S. Chenais, F. Druon, F. Balembois, G. Lucas-Leclin, Y. Fichot, P. Georges, R. Gaume, B. Viana, G. Aka, D. Vivien, Thermal lensing measurements in diode-pumped Yb-doped GdCOB, YCOB, YSO, YAG and KGW. *Opt. Mater.* **22**(2), 129–137 (2003)
21. V.V. Zelenogorsky, A.A. Solovyov, I.E. Kozhevator, E.E. Kamenetsky, E.A. Rudenchik, O.V. Palashov, D.E. Silin, E.A. Khazanov, High-precision methods and devices for in situ measurements of thermally induced aberrations in optical elements. *Appl. Opt.* **45**(17), 4092–4101 (2006)
22. Z. Zhu, Y. Li, J. Chen, J. Ma, J. Chu, Development of a unimorph deformable mirror with water cooling. *Opt. Express* **25**(24), 29916–29926 (2017)
23. T. Peng, C. Dai, J. Lou, Y. Cui, B. Tao, J. Ma, A low-cost deformable lens for correction of low-order aberrations. *Opt. Commun.* **460**, 125209 (2020)
24. S. Piehler, T. Dietrich, P. Wittmüss, O. Sawodny, M.A. Ahmed, T. Graf, Deformable mirrors for intra-cavity use in high-power thin-disk lasers. *Opt. Express* **25**(4), 4254–4267 (2017)
25. H. Nadgaran, M. Servatkah, The effects of induced heat loads on the propagation of Ince-Gaussian beams. *Opt. Commun.* **284**(22), 5329–5337 (2011)
26. M.-M. Zhang, S.-C. Bai, J. Dong, Effects of Cr⁴⁺ ions on forming Ince-Gaussian modes in passively Q-switched microchip solid-state lasers. *Laser Phys. Lett.* **16**(2), 025003 (2019)
27. H. Nadgaran, R. Fallah, Investigation of the pump reshaping effect on the thermally-affected Helmholtz-gauss beams generated by a solid-state laser. *Laser Phys.* **25**(8), 085007 (2015)
28. M. Sabaiean, H. Nadgaran, Bessel-Gauss beams: investigations of thermal effects on their generation. *Opt. Commun.* **281**(4), 672–678 (2008)
29. M. Gerber, T. Graf, A. Kudryashov, Generation of custom modes in a Nd:YAG laser with a semipassive bimorph adaptive mirror. *Appl. Phys. B* **83**(1), 43–50 (2006)
30. T.Y. Cherezova, L.N. Kaptsov, A.V. Kudryashov, Cw industrial rod YAG: Nd³⁺ laser with an intracavity active bimorph mirror. *Appl. Opt.* **35**(15), 2554–2561 (1996)
31. T.Y. Cherezova, S. Chesnokov, L. Kaptsov, A. Kudryashov, Super-Gaussian laser intensity output formation by means of adaptive optics. *Opt. Commun.* **155**(1–3), 99–106 (1998)
32. T.Y. Cherezova, S.S. Chesnokov, L.N. Kaptsov, V.V. Samarkin, A.V. Kudryashov, Active laser resonator performance: formation

- of a specified intensity output. *Appl. Opt.* **40**(33), 6026–6033 (2001)
33. W. Lubeigt, G. Valentine, J. Girkin, E. Bente, D. Burns, Active transverse mode control and optimisation of an all-solid-state laser using an intracavity adaptive-optic mirror. *Opt. Express* **10**(13), 550–555 (2002)
 34. W. Lubeigt, M. Griffith, L. Laycock, D. Burns, Reduction of the time-to-full-brightness in solid-state lasers using intra-cavity adaptive optics. *Opt. Express* **17**(14), 12057–12069 (2009)
 35. D. Kim, S. Noh, S. Ahn, J. Kim, Influence of a ring-shaped pump beam on temperature distribution and thermal lensing in end-pumped solid state lasers. *Opt. Express* **25**(13), 14668–14675 (2017)
 36. D. Lin, W. Clarkson, Reduced thermal lensing in an end-pumped Nd:YVO₄ laser using a ring-shaped pump beam, in *CLEO: Science and Innovations*. Optical Society of America, SM3M–5 (2016)
 37. T. Omatsu, K. Miyamoto, A.J. Lee, Wavelength-versatile optical vortex lasers. *J. Opt.* **19**(12), 123002 (2017)
 38. A. Forbes, Controlling light's helicity at the source: orbital angular momentum states from lasers. *Philos. Trans. R. Soc. A* **375**(2087), 20150436 (2017)
 39. Z. Fang, K. Xia, Y. Yao, J. Li, Radially polarized LG⁰¹-mode Nd:YAG laser with annular pumping. *Appl. Phys. B* **117**(1), 219–224 (2014)
 40. Z. Fang, K. Xia, Y. Yao, J. Li, Radially polarized and passively Q-switched Nd:YAG laser under annular-shaped pumping. *IEEE J. Sel. Top. Quantum Electron.* **21**(1), 337–342 (2014)
 41. T. Dietrich, M. Rumpel, T. Graf, M.A. Ahmed, Investigations on ring-shaped pumping distributions for the generation of beams with radial polarization in an Yb:YAG thin-disk laser. *Opt. Express* **23**(20), 26651–26659 (2015)
 42. F. Brandt, M. Hiekkamäki, F. Bouchard, M. Huber, R. Fickler, High-dimensional quantum gates using full-field spatial modes of photons. *Optica* **7**(2), 98–107 (2020)
 43. A. Forbes, I. Nape, Quantum mechanics with patterns of light: Progress in high dimensional and multidimensional entanglement with structured light. *AVS Quantum Sci.* **1**(1), 011701 (2019)
 44. A. Forbes, Structured light from lasers. *Laser Photonics Rev.* **13**(11), 1900140 (2019)
 45. C. Rosales-Guzmán, B. Ndagano, A. Forbes, A review of complex vector light fields and their applications. *J. Opt.* **20**(12), 123001 (2018). [Online]. <http://iopscience.iop.org/article/10.1088/2040-8986/aeab7d>
 46. H. Rubinsztein-Dunlop, A. Forbes, M.V. Berry, M.R. Dennis, D.L. Andrews, M. Mansuripur, C. Denz, C. Alpmann, P. Banzer, T. Bauer et al., Roadmap on structured light. *J. Opt.* **19**(1), 013001 (2016)
 47. D. Kim, J. Kim, High-power TEM⁰⁰ and Laguerre-Gaussian mode generation in double resonator configuration. *Appl. Phys. B* **121**(3), 401–405 (2015)
 48. M.L. Lukowski, J.T. Meyer, C. Hessenius, E.M. Wright, M. Fallahi, Generation of high-power spatially structured beams using vertical external cavity surface emitting lasers. *Opt. Express* **25**(21), 25504–25514 (2017)
 49. P. Tuan, Y. Hsieh, Y. Lai, K. Huang, Y. Chen, Characterization and generation of high-power multi-axis vortex beams by using off-axis pumped degenerate cavities with external astigmatic mode converter. *Opt. Express* **26**(16), 20481–20491 (2018)
 50. M. Eckler, F. Beirrow, T. Dietrich, F. Schaal, C. Pruss, W. Osten, N. Aubry, M. Perrier, J. Didierjean, X. Délen et al., High-power single-stage single-crystal Yb: YAG fiber amplifier for radially polarized ultrashort laser pulses. *Appl. Phys. B* **123**(5), 139 (2017)
 51. J. Kim, J. Mackenzie, J. Hayes, W. Clarkson, High power Er:YAG laser with radially-polarized Laguerre-Gaussian (LG⁰¹) mode output. *Opt. Express* **19**(15), 14526–14531 (2011)
 52. M. Okida, T. Omatsu, M. Itoh, T. Yatagai, Direct generation of high power Laguerre-Gaussian output from a diode-pumped Nd:YVO₄ 1.3- μ m bounce laser. *Opt. Express* **15**(12), 7616–7622 (2007)
 53. J.-P. Negel, A. Loescher, B. Dannecker, P. Oldorf, S. Reichel, R. Peters, M.A. Ahmed, T. Graf, Thin-disk multipass amplifier for fs pulses delivering 400 W of average and 2.0 GW of peak power for linear polarization as well as 235 W and 1.2 GW for radial polarization. *Appl. Phys. B* **123**(5), 156 (2017)
 54. R.-G. Carmelo, H. Xiao-Bo, S. Adam, P. Moreno-Acosta, S. Franke-Arnold, R. Ramos-Garcia, A. Forbes, Polarisation-insensitive generation of complex vector modes from a digital micromirror device. *Sci. Rep.* **10**(1), 1–9 (2020)
 55. W. Liu, J. Fan, C. Xie, Y. Song, C. Gu, L. Chai, C. Wang, M. Hu, Programmable controlled mode-locked fiber laser using a digital micromirror device. *Opt. Lett.* **42**(10), 1923–1926 (2017)
 56. H. Messaoudi, F. Thiemicke, C. Falldorf, R.B. Bergmann, F. Vollertsen, Distortion-free laser beam shaping for material processing using a digital micromirror device. *Prod. Eng.* **11**(3), 365–371 (2017)
 57. K.J. Mitchell, S. Turtaev, M.J. Padgett, T. Čížmár, D.B. Phillips, High-speed spatial control of the intensity, phase and polarisation of vector beams using a digital micro-mirror device. *Opt. Express* **24**(25), 29269–29282 (2016)
 58. X. Ding, Y. Ren, R. Lu, Shaping super-Gaussian beam through digital micro-mirror device. *Sci. China Phys. Mech. Astron.* **58**(3), 1–6 (2015)
 59. Y.-X. Ren, Z.-X. Fang, L. Gong, K. Huang, Y. Chen, R.-D. Lu, Dynamic generation of Ince-Gaussian modes with a digital micromirror device. *J. Appl. Phys.* **117**(13), 133106 (2015)
 60. Y.-X. Ren, R.-D. Lu, L. Gong, Tailoring light with a digital micromirror device. *Ann. Phys.* **527**(7–8), 447–470 (2015)
 61. Y.-X. Ren, Z.-X. Fang, L. Gong, K. Huang, Y. Chen, R.-D. Lu, Digital generation and control of Hermite-Gaussian modes with an amplitude digital micromirror device. *J. Opt.* **17**(12), 125604 (2015)
 62. L. Gong, Y. Ren, W. Liu, M. Wang, M. Zhong, Z. Wang, Y. Li, Generation of cylindrically polarized vector vortex beams with digital micromirror device. *J. Appl. Phys.* **116**, 183105 (2014)
 63. F. Schepers, T. Bexter, T. Hellwig, C. Fallnich, Selective Hermite-Gaussian mode excitation in a laser cavity by external pump beam shaping. *Appl. Phys. B* **125**(5), 75 (2019)
 64. X. Hu, Q. Zhao, P. Yu, X. Li, Z. Wang, Y. Li, L. Gong, Dynamic shaping of orbital-angular-momentum beams for information encoding. *Opt. Express* **26**(2), 1796–1808 (2018)
 65. A.O. Georgieva, A.V. Belashov, N.V. Petrov, Complex wavefront manipulation and holographic correction based on digital, in *Emerging Digital Micromirror Device Based Systems and Applications XII*, 11294. International Society for Optics and Photonics, 112940B (2020)
 66. M.A. Cox, E. Toninelli, L. Cheng, M.J. Padgett, A. Forbes, A high-speed, wavelength invariant, single-pixel wavefront sensor with a digital micromirror device. *IEEE Access* **7**, 85860–85866 (2019)
 67. Y. Chen, Z.-X. Fang, Y.-X. Ren, L. Gong, R.-D. Lu, Generation and characterization of a perfect vortex beam with a large topological charge through a digital micromirror device. *Appl. Opt.* **54**(27), 8030–8035 (2015)
 68. J. Di, Y. Yu, Z. Wang, W. Qu, C.Y. Cheng, J. Zhao, Quantitative measurement of thermal lensing in diode-side-pumped Nd:YAG laser by use of digital holographic interferometry. *Opt. Express* **24**(25), 28185–28193 (2016)
 69. S. Scholes, R. Kara, J. Pinnell, V. Rodríguez-Fajardo, A. Forbes, Structured light with digital micromirror devices: a guide to best practice. *Opt. Eng.* **59**(4), 041202 (2019)

70. A. Manthalkar, I. Nape, N.T. Bordbar, C. Rosales-Guzmán, S. Bhattacharya, A. Forbes, A. Dudley, All-digital stokes polarimetry with a digital micromirror device. *Opt. Lett.* **45**(8), 2319–2322 (2020)
71. B. Zhao, X.-B. Hu, V. Rodríguez-Fajardo, A. Forbes, W. Gao, Z.-H. Zhu, C. Rosales-Guzmán, Determining the non-separability of vector modes with digital micromirror devices. *Appl. Phys. Lett.* **116**(9), 091101 (2020)
72. K. Singh, N. Tabebordbar, A. Forbes, A. Dudley, Digital stokes polarimetry and its application to structured light: tutorial. *JOSA A* **37**(11), C33–C44 (2020)
73. W.-H. Lee, Binary computer-generated holograms. *Appl. Opt.* **18**(21), 3661–3669 (1979)
74. M. Mirhosseini, O.S. Magana-Loaiza, C. Chen, B. Rodenburg, M. Malik, R.W. Boyd, Rapid generation of light beams carrying orbital angular momentum. *Opt. Express* **21**(25), 30196–30203 (2013)
75. A. Jesacher, A. Schwaighofer, S. Fürhapter, C. Maurer, S. Bernet, M. Ritsch-Marte, Wavefront correction of spatial light modulators using an optical vortex image. *Opt. Express* **15**(9), 5801–5808 (2007)
76. T. Čižmár, M. Mazilu, K. Dholakia, In situ wavefront correction and its application to micromanipulation. *Nat. Photonics* **4**(6), 388–394 (2010)
77. S. Turtaev, I.T. Leite, K.J. Mitchell, M.J. Padgett, D.B. Phillips, T. Čižmár, Comparison of nematic liquid-crystal and DMD based spatial light modulation in complex photonics. *Opt. Express* **25**(24), 29874–29884 (2017)
78. E. Bernhardt, A. Forbes, C. Bollig, M.D. Esser, Estimation of thermal fracture limits in quasi-continuous-wave end-pumped lasers through a time-dependent analytical model. *Opt. Express* **16**(15), 11115–11123 (2008)
79. D. Wright, Beamwidths of a diffracted laser using four proposed methods. *Opt. Quantum Electron.* **24**(9), S1129–S1135 (1992)
80. D. Wright, P. Greve, J. Fleischer, L. Austin, Laser beam width, divergence and beam propagation factor? an international standardization approach. *Opt. Quantum Electron.* **24**(9), S993–S1000 (1992)
81. A. Siegman, Standard of the measurement of beam widths, beam divergence and propagation factors, Proposal for a working draft ISO TC 172 SC9/WG1 (1990)
82. J.F. Ready, *Industrial Applications of Lasers* (Elsevier, Amsterdam, 1997)
83. P. Shukla, J. Lawrence, A. Paul et al., Influence of laser beam brightness during surface treatment of a ZrO₂ engineering ceramic. *Lasers Eng.* **22**(3), 151 (2012)
84. P. Shukla, J. Lawrence, Y. Zhang, Understanding laser beam brightness: a review and new prospective in material processing. *Opt. Laser Technol.* **75**, 40–51 (2015)

Publisher's Note Springer Nature remains neutral with regard to jurisdictional claims in published maps and institutional affiliations.